Experimental and Theoretical Studies of Sodium Cation Interactions with D-Arabinose, Xylose, Glucose, and Galactose

A. L. Heaton and P. B. Armentrout*

Department of Chemistry, University of Utah, Salt Lake City, Utah 84112

Received: May 9, 2008; Revised Manuscript Received: July 18, 2008

The binding of Na^+ to arabinose (Ara), xylose (Xyl), glucose (Glc), and galactose (Gal) is examined in detail by studying the collision-induced dissociation (CID) of the four sodiated monosaccharide complexes with Xe using a guided ion beam tandem mass spectrometer (GIBMS). Analysis of the energy-dependent CID cross-sections provides 0 K sodium cation affinities for experimental complexes after accounting for unimolecular decay rates, internal energy of reactant ions, and multiple ion-neutral collisions. Quantum chemical calculations for a number of geometric conformations of each Na^+(L) complex with a comprehensive analysis of the α and β anomeric forms are determined at the B3LYP/6−311+G(d,p) level with single-point energies calculated at MP2(full), B3LYP, and B3P86 levels using a 6−311+G(2d,2p) basis set. This coordinated examination of both experimental work and quantum chemical calculations allows for determination of the bond energy for both the α and β forms of each monosaccharide studied here. An understanding of the energetic contributions of individual structural characteristics as well as the energetic trends in binding among the monosaccharides is developed. Structural characteristics that affect the energetics of binding involve multidentate sodium cation coordination, ring sterics, and hydrogen bonding schemes. The overall trend in sodium binding affinities for the eight ligands follows β-Ara < α-Ara < β-Xyl < β-Glc < α-Glc < α;-Xyl < α-Gal < β-Gal.

Introduction

The biological roles of carbohydrates are abundant and diverse.[1,2] One key role that carbohydrates play in molecular functioning is to act as a biological code in cellular recognition and signaling processes by combining with proteins and lipids on cell surfaces. Their low threshold for conformational modification allows them to exist in a multitude of functional conformers and act as an "alphabet" in cell-to-cell recognition. Yet complexation of the carbohydrates to metal cations reduces their conformational flexibility and locks them into characteristic geometries. Thus, the intramolecular properties of metal−carbohydrate systems are of significant interest.

Experimental work utilizing gas-phase threshold collision-induced dissociation (TCID) is ideal for such intramolecular characterizations because complications resulting from solvent effects can be eliminated. Furthermore, the measurement of gas-phase cation affinities is convenient and reflects the intrinsic bond strengths within alkali metal cation−carbohydrate systems for direct comparison with theoretical results. Our laboratory[3−7] and others[8−14] have used this methodology to understand the binding affinity of metal ions with small-scale systems to generate a "thermodynamic vocabulary" of specific alkali metal binding interactions useful in understanding systems of greater complexity.[15]

The majority of studies on cationized carbohydrates have been used for elucidation of the structural characteristics of complex glycans, including determination of linkage, branching modes, and anomeric identity of constituent monosaccharides.[16−19] Recent attention has been focused on negative ion fragmentation of saccharide complexes, as these methods provide additional structural details of monosaccharides and oligosaccharides.[20−24] Some experimental data on sodium cation affinities for monosaccharides are available. Wesdemiotis and co-workers[25] determined sodium cation affinities of select pentoses, hexoses, and disaccharides using Cooks's kinetic method[26,27] based on the dissociation characteristics of collisionally activated Na^+ heterodimer complexes consisting of the saccharide ligand and reference base. The kinetic method measures relative free energies of dissociation of the two ligands to estimate the difference in binding, which is converted to absolute saccharide bond dissociation energies (BDEs) by anchoring to known $\Delta H°_{298}(Na^+\text{-base})$ values. Quantitative results of this study for the arabinose (Ara), xylose (Xyl), glucose (Glc), and galactose (Gal) saccharides studied here are discussed further below. No direct measurements of Na^+ binding to these monosaccharides have been accomplished previously.

The present study examines sodium cation complexes of the monosaccharides Ara, Xyl, Glc, and Gal experimentally in a guided ion beam mass spectrometer (GIBMS). Na^+(L) ions are generated in an electrospray ionization source directly from solution phase, where the monosaccharide ligands exist in two anomeric forms, α and β. Therefore, the relative abundance of the two forms in our gas-phase Na^+(α-L) and Na^+(β-L) experimental complexes should approximately match that of the ligands under aqueous conditions, given further considerations discussed below. Interestingly, the ground state α and β forms of each ligand bind Na^+ in distinctively different geometries, which are characterized here by quantum chemical calculations. Theoretical results for both anomeric forms are compared to modeled 0 K experimental thresholds for analysis.

We provide here the first directly measured experimental values for Na^+ binding with Ara, Xyl, Glc, and Gal. Absolute BDEs of the Na^+(L) complexes are measured using TCID in a guided ion beam tandem mass spectrometer. Theoretical calculations at the B3LYP/6−311+G(d,p) level are carried out to provide structures, vibrational frequencies, and rotational constants needed for analysis of the TCID data. These BDEs are compared to theoretical calculations performed for a number of possible Na^+(L) geometries at the MP2(full)/6−311+G(2d,2p),

10.1021/jp804113q CCC: $40.75
Published on Web 09/18/2008

B3LYP/6−311+G(2d,2p), and B3P86/6−311+G(2d,2p) levels using geometries and zero point energy corrections calculated at the B3LYP/6−311+G(d,p) level of theory. Calculations at this level also provide the difference in binding energies between anomers, $\Delta D_0(Na^+\text{-L})$, used to determine $D_0(Na^+\text{-L})$ for the α and β forms of each monosaccharide studied here.

Experimental and Computational Section

General Experimental Procedures. Cross-sections for CID of the metal−ligand complexes are measured using a guided ion beam tandem mass spectrometer that has been described in detail previously.[28,29] Studies of each Na^+(L) complex are conducted using an electrospray ionization (ESI) source[30] under conditions similar to those described previously.[30] Briefly, the ESI is operated using a 50:50 by volume H_2O/MeOH solution with ~10^{-4} M monosaccharide and NaCl (all chemicals purchased from Sigma-Aldrich), which is syringe-pumped at a rate of 0.04 mL/h into a 35 gauge stainless steel needle biased at ~2000 V. Ionization occurs over the ~5 mm distance from the tip of the needle to the entrance of the capillary, biased at ~35 V. Ions are directed by a capillary heated to 80 °C into a radiofrequency (rf) ion funnel,[31] wherein they are focused into a tight beam. Ions exit the ion funnel and enter an rf hexapole ion guide that traps them radially. Here the ions undergo multiple collisions (> 10^4) with the ambient gas and become thermalized.

The ESI source is assumed to produce ions having their internal energies well described by a Maxwell−Boltzmann distribution of rovibrational states at 300 K, as characterized in previous experiments.[30,32] Metal−ligand complexes are then extracted from the source and mass selected using a magnetic momentum analyzer. The mass selected ions are decelerated to a well-defined kinetic energy and are focused into a rf octopole ion guide that traps the ions radially.[33,34] The ion guide minimizes losses of the reactant and any product ions resulting from scattering. The octopole passes through a static gas cell containing xenon, which is used as the collision gas for reasons described elsewhere.[35,36] After collision, the reactant and product ions drift to the end of the octopole where they are extracted and focused into a quadrupole mass filter for mass analysis. The ions are detected with a high voltage dynode, scintillation ion detector,[37] and the signal is processed using standard pulse counting techniques. Ion intensities, measured as a function of collision energy, are converted to absolute cross-sections as described previously.[28] The uncertainty in relative cross-sections is about ±5% and that for the absolute cross-sections is about ±20%. The ion kinetic energy distribution is measured to be Gaussian and has a typical fwhm of 0.1−0.2 eV (laboratory) for the ESI source. Uncertainties in the absolute energy scale are about ±0.05 eV (laboratory). Ion kinetic energies in the laboratory frame are converted to energies in the center-of-mass (CM) frame using $E_{CM} = E_{lab}\, m/(m + M)$, where M and m are the masses of the ionic and neutral reactants, respectively. All energies herein are reported in the CM frame unless otherwise noted.

Thermochemical Analysis. Threshold regions of the CID reaction cross-sections are modeled using eq 1,

$$\sigma(E) = (n\sigma_0/E)\sum g_i \int_{E_0-E_i}^{E} (1 - e^{-k(E^*)\tau})(E-\varepsilon)^{n-1} \mathrm{d}(\varepsilon) \quad (1)$$

where σ_0 is an energy-independent scaling factor, n is an adjustable parameter that describes the efficiency of collisional energy transfer,[29] E is the relative kinetic energy of the reactants, E_0 is the threshold for dissociation of the ground electronic and rovibrational state of the reactant ion at 0 K, τ is the experimental time for dissociation (~5×10^{-4} s in the extended dual octopole configuration as measured by time-of-flight studies),[29] ε is the energy transferred from translation during the collision, and E^* is the internal energy of the energized molecule (EM) after the collision, i.e., $E^* = \varepsilon + E_i$. The summation is over the rovibrational states of the reactant ions, i, where E_i is the excitation energy of each state and g_i is the fractional population of those states ($\sum g_i = 1$). The Beyer−Swinehart algorithm[38−40] is used to evaluate the number and density of the rovibrational states, and the relative populations g_i are calculated for a Maxwell−Boltzmann distribution at 300 K.

The term $k(E^*)$ is the unimolecular rate constant for dissociation of the energized molecule and is defined by Rice−Ramsperger−Kassel−Marcus (RRKM) theory as in eq 2,[41,42]

$$k(E^*) = dN^{\dagger}_{vr}(E^* - E_0)/h\rho_{vr}(E^*) \quad (2)$$

where d is the reaction degeneracy, $N^{\dagger}_{vr}$ ($E^* - E_0$) is the sum of rovibrational states of the transition state (TS) at an energy $E^* - E_0$, and $\rho_{vr}(E^*)$ is the density of states of the energized molecule (EM) at the available energy, E^*. These rate constants allow kinetic shifts to be modeled as discussed below.[43,44]

Several effects that obscure the interpretation of the data must be accounted for during data analysis in order to produce accurate thermodynamic information. The first effect involves energy broadening resulting from the thermal motion of the neutral collision gas and the kinetic energy distribution of the reactant ion. This is accounted for by explicitly convoluting the model over both kinetic energy distributions, as described elsewhere in detail.[28] The second effect considers that eq 1 only models cross-sections that represent products formed as the result of a single collision event. To ensure rigorous single collision conditions, data are collected at three pressures of Xe, generally about 0.16, 0.08, and 0.04 mTorr, and the resulting cross-sections evaluated for pressure effects and extrapolated to zero pressure.[45] The third effect arises from the lifetime for dissociation. As the size of reactant molecules increases, so do the number of vibrational modes of the reactant ion and thus the time for energy randomization into the reaction coordinate after collision. Thus, some energized molecules may not dissociate during the time scale of the experiment.[43] This leads to a delayed onset for the CID threshold, a kinetic shift, which becomes more noticeable as the size of the molecule increases. These kinetic shifts are estimated by the incorporation of RRKM theory as shown in eq 1 and as described in detail elsewhere.[43] To evaluate the rate constant in eq 1, sets of rovibrational frequencies for the EM and all TSs are required. Because the metal−ligand interactions in our Na^+(L) complexes are mainly electrostatic, the most appropriate model for the TS for dissociation of the intact ligand is a loose association of the ion and neutral ligand fragments. The appropriateness of this assumption for multidentate ligands has been verified previously for crown ethers[7,46] and more recently for the tripeptide, GlyGlyGly.[32] Therefore, these TSs are treated as product-like, such that the TS frequencies are those of the dissociation products. The molecular parameters needed for the RRKM calculation are taken from the quantum chemical calculations detailed in the next section. The transitional frequencies in the TSs are treated as rotors, a treatment that corresponds to a phase space limit (PSL), as described in detail elsewhere.[43,44] The 2D external rotations are treated adiabatically but with centrifugal effects included.[40] In the present work, the adiabatic 2D rotational energy is treated using a statistical distribution with an explicit summation over all the possible values of the rotational quantum number.[43,44] We additionally determine the entropy of activation for each

dissociation channel as described in detail elsewhere.[44] These $\Delta S^{\ddagger}$ quantities, which are energy (or temperature) dependent, are tabulated at 1000 K.

The model cross-sections of eq 1 are convoluted with the kinetic energy distribution of the reactants and compared to the data. A nonlinear least-squares analysis is used to provide optimized values for σ_0, n, and E_0. The uncertainty associated with E_0 is estimated from the range of threshold values determined from different data sets with variations in the parameter n, variations in vibrational frequencies (±10% in most frequencies and a factor of 2 for the $Na^+(L)$ modes), changes in τ by factors of 2, and the uncertainty of the absolute energy scale, 0.05 eV (laboratory).

In deriving the final optimized BDEs at 0 K, two assumptions are made. First, we assume that there is no activation barrier in excess of the reaction endothermicity for the loss of the ligand, which is generally true for ion−molecule reactions and for the heterolytic noncovalent bond dissociations considered here.[47] Second, the measured threshold E_0 values for dissociation are from ground-state reactant to ground-state ion and neutral ligand products. Given the relatively long experimental time frame (~5×10^{-4} s), dissociating products should be able to rearrange to their low energy conformations after collisional excitation.

Computational Details. Computational analyses of the neutral ligands studied here have been well-characterized previously,[48−50] as discussed further below. For the metalated complexes of interest, a number of geometric conformations with relative energies close to the lowest energy complex are probable. To find the global minimum energy and all low-energy geometries, a large number of possible conformations were screened as follows.[51] A simulated annealing methodology using the AMBER suite of programs and the AMBER force field[52] was used to generate starting structures for higher level optimizations. For the pentose (Ara and Xyl) and hexose (Glc and Gal) complexes studied here, temperature-ramping conditions for the simulated annealing necessary to explore all available conformational space resulted in formation of all possible D and L isomeric conformations and α and β anomeric conformations, as well as formation of all possible monosaccharides within the pentose and hexose systems. Because of the number of structural variants generated, multiple annealing runs were performed for both the pentoses and hexoses (~5 runs each with variant ramping conditions, each generating 1000 structures) until no new conformations were generated. All the unique structures were further optimized using Nwchem[53] at the HF/3−21G level. We have found for similar complexes that energies determined with this low-level ab initio calculation show a higher correlation with energies calculated at higher levels of theory than the relative energies from the AMBER force field. At this point, all unique structures were evaluated for identity. Conformational L isomers were discarded, and all structures corresponding to the α and β anomeric conformations of Ara, Xyl, Glc, and Gal were categorized. All low-energy structures for each of the eight complexes from the HF/3−21G calculations within 30 or more kJ/mol of the lowest energy structure (20−30 structures for each $Na^+(L)$ complex) were further optimized using Gaussian 03[54] at the B3LYP/6−31G(d) level with "loose" optimization (maximum step size of 0.01 au and an rms force of 0.0017 au) to facilitate more rapid convergence. All unique structures (11−20 structures for each complex) were then optimized at the B3LYP/6−311+G(d,p) level. Rotational constants were obtained from the optimized structures and vibrational frequencies were also calculated at this level. When used in internal energy determinations or for RRKM calculations, the vibrational frequencies were scaled by 0.99.[55] Single-point energies were calculated at the MP2(full), B3LYP, and B3P86 levels using the 6−311+G(2d,2p) basis set and the B3LYP/6−311+G(d,p) geometries. Ground state structures for the neutral monosaccharides studied here were optimized at calculated and the same levels. Zero-point vibrational energy (ZPE) corrections in the BDEs were determined using the scaled vibrational frequencies. Basis set superposition errors (BSSE) in the BDEs were estimated using the full counterpoise (cp) method.[56,57] For the MP2 single-point energies, the BSSE corrections range from 12−16 kJ/mol, whereas for the B3LYP and B3P86 single-point energies, they range between 3−5 kJ/mol for all structures examined here. This is consistent with previous observations by this laboratory[3,51] and others[58] that BSSE corrections for DFT calculations on alkali metal cation systems are generally small. Feller and co-workers[59,60] and Ohannesian and co-workers[9,10] have previously commented that the full counterpoise approximation to BSSE can provide worse agreement with experiment than theoretical values without BSSE corrections. Because of this possibility for BSSE to overcorrect the MP2 calculations, the "best" MP2 values may fall between the MP2 values with and without BSSE corrections. Therefore, both values are reported here. All of the absolute binding energies obtained using DFT calculations reported here include BSSE corrections.

Results

Cross-Sections for Collision-Induced Dissociation. Kinetic energy dependent experimental cross-sections were obtained for the interaction of Xe with $Na^+(L)$ where L = Ara, Xyl, Glc, and Gal. Figure 1 shows representative pressure-extrapolated cross-sections for all four $Na^+(L)$ systems from data collected at xenon pressures of ~0.04, 0.08, and 0.16 mTorr. Over the energies evaluated here, the only process observed for each complex is the loss of the intact ligand in the collision-induced dissociation (CID) reaction 3.

$$Na^+(L) + Xe \rightarrow Na^+ + L + Xe \qquad (3)$$

The model of eq 1 was used to analyze the thresholds for reaction 3 for the four $Na^+(L)$ systems, and the resulting optimized fitting parameters obtained are listed in Table 1. Each cross-section was fit using parameters for the reaction of both the alpha and beta conformers, although the threshold energies change by ≤1 kJ/mol in all cases. Table 1 reports the average of these analyses with experimental uncertainties that include these minor effects. Further discussion regarding our experimental sensitivity to the abundances of the different monosaccharide anomeric conformers is provided below.

Figure 1 shows that all experimental cross-sections are reproduced by eq 1 over a large range of energies (~3 eV) and magnitudes (over 2 orders of magnitude). Modest kinetic shifts are observed and range from about 0.4 eV for the pentose systems to almost 0.8 eV for the most strongly bound $Na^+(Gal)$ complex. This trend is consistent with previous observations that kinetic shifts track with increasing threshold energy and ligand complexity. From our analyses, we also derive values of $\Delta S^{\ddagger}_{1000}$, the entropy of activation at 1000 K, which give some idea of the looseness of the transition states. These values, listed in Table 1, are in the range determined by Lifshitz[61] for simple bond cleavage dissociations. This is reasonable considering that the TS is assumed to lie at the centrifugal barrier for the association of $Na^+ + L$. The rotational contributions to $\Delta S^{\ddagger}_{1000}$ are fairly constant for the complexes studied here. The moderate variations observed in the $\Delta S^{\ddagger}_{1000}$ values are the result of vibrational contributions from the different TS geometries.

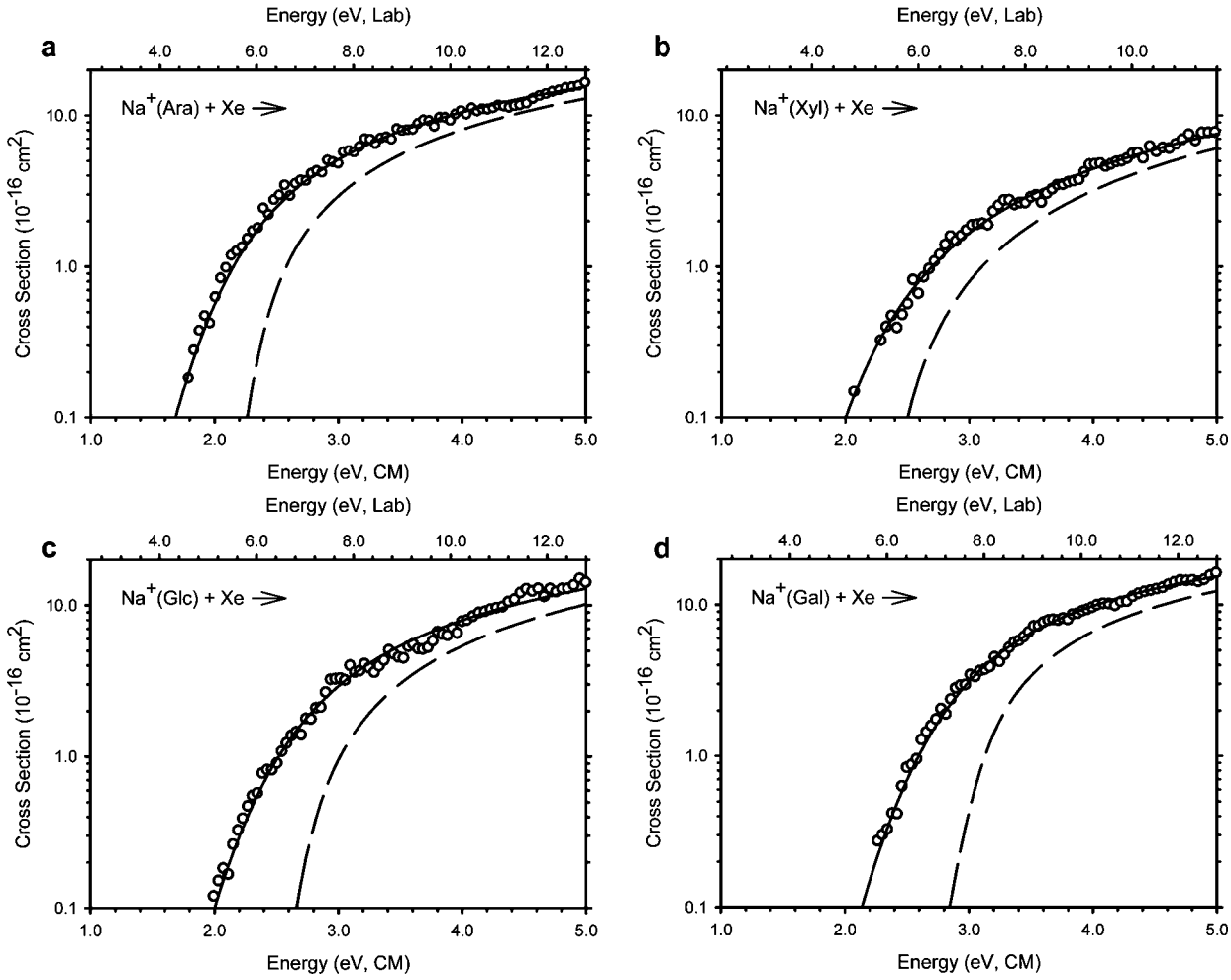

Figure 1. Cross-sections for collision-induced dissociation of $Na^+(L)$, where L = D-arabinose, xylose, glucose, and galactose (parts a−d, respectively), with Xe as a function of kinetic energy in the center-of-mass frame (lower *x*-axis) and the laboratory frame (upper *x*-axis). Solid lines show the best fit to the data using the model of eq 1 convoluted over the neutral and ion kinetic and internal energy distributions. Dashed lines show the model cross-sections in the absence of experimental kinetic energy broadening for reactants with an internal energy of 0 K.

TABLE 1: Fitting Parameters of Eq 1, Threshold Dissociation Energies at 0 K, and Entropies of Activation at 1000 K for CID of $Na^+(L)$[a]

reactant	σ_0	n	E_0 (eV), no RRKM	E_0 (PSL)[b] (eV)	$\Delta S^{\ddagger}_{1000}$ (J/K/mol)
Na^+(Ara)	1.34 (1.0)	1.6 (0.1)	2.21 (0.05)	1.77 (0.06)	31 (2)
Na^+(Xyl)	4.78 (0.6)	1.9 (0.1)	2.30 (0.06)	1.88 (0.06)	54 (2)
Na^+(Glc)	13.8 (0.8)	1.6 (0.1)	2.62 (0.05)	1.88 (0.07)	53 (2)
Na^+(Gal)	2.52 (1.4)	1.3 (0.1)	2.89 (0.05)	2.10 (0.07)	50 (2)

[a] Uncertainties in parentheses. [b] The phase space limit (PSL) assumes that all transition states for dissociation are product-like and located at the centrifugal barrier, providing the "best" values that are corrected for kinetic shifts and used in subsequent discussions.

Theoretical Results for Sodiated Monosaccharide Complexes. Structures of the four neutral monosaccharides experimentally studied here have been calculated previously. Kenttämaa and co-workers[48] determined the ground state (GS) structures for α and β arabinose and xylose at the B3LYP/6−311+G(d,p) level of theory from starting structures generated by using molecular mechanics and semiempirical methods. Barrows et al.[49] determined the GS structures of α and β glucose using 14 different levels of theory from structures generated using molecular mechanics simulations. Lastly, Rahal-Sekkal et al.[50] determined the GS structures of α and β galactose at the RHF/6−31G* level of theory based on X-ray crystallographic data as well as known low-energy structural characteristics of galactose analogues.

We obtained parameters for each of the eight GS structures determined from these studies and optimized them at the B3LYP/6−311+G(d.p) level with single point energies determined at the B3LYP, B3P86, and MP2(full) levels using the 6−311+G(2d,2p) basis set. The optimized structures are provided in Figure 2. The relative energies between the anomeric forms (the anomeric effect) including zero point energy effects are provided in Table 2.

Our results provide an anomeric effect for Ara and Xyl of 4.3−6.7 kJ/mol and 1.9−3.8 kJ/mol, respectively, consistent with results from Kenttämaa and co-workers[48] determined at a comparable level of theory, 4.6 and 2.1 kJ/mol, respectively. In contrast, Rahal-Sekkal et al.[50] found an anomeric effect for Gal of 8.3 kJ/mol at the RHF/6−31G* level, whereas our calculations find an anomeric effect of −0.2−2.5 kJ/mol. This discrepancy is presumably a consequence of the much lower level of theory (without electron correlation) used by Rahal-Sekkal et al. Consistent with these variations are the results of Barrows et al.[49] for Glc, where 14 different levels of theory provided an anomeric effect ranging from −1.7−16.3 kJ/mol. Clearly the different levels of theory can vary widely in their description of anomericity. Their MP2/cc-pVDZ//HF/cc-pVDZ value, 3.3 kJ/mol, is closest to our calculated range of 1.8−3.6 kJ/mol.

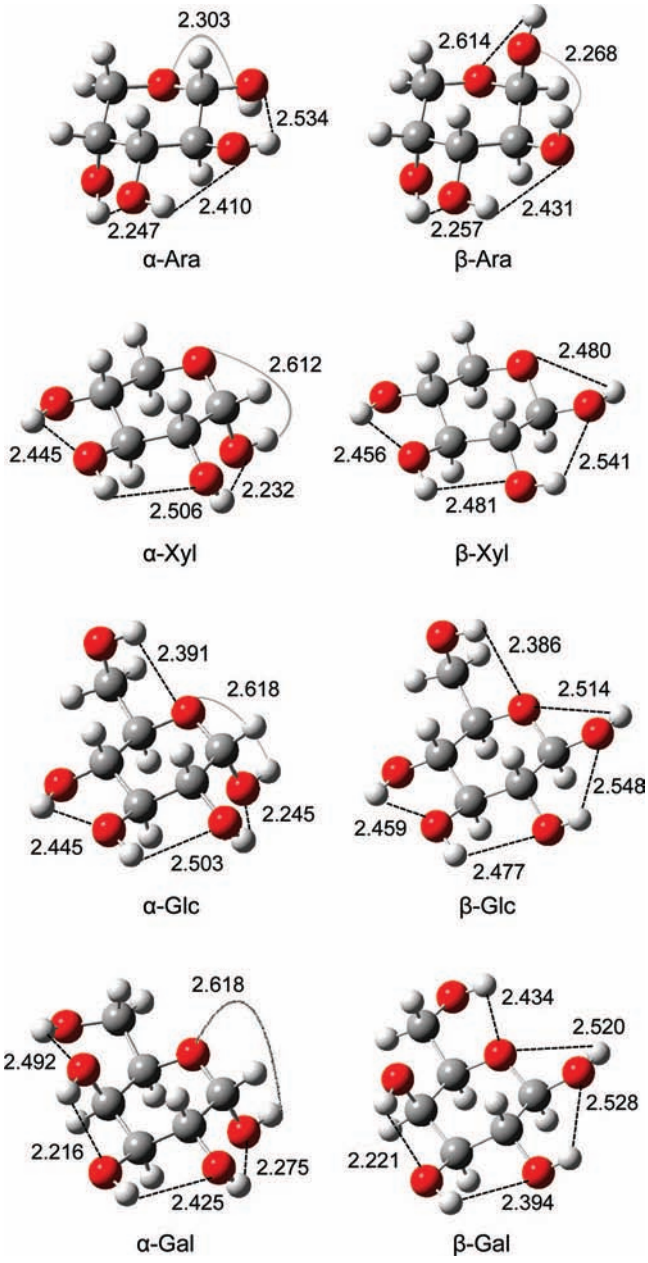

Figure 2. Ground state conformations of neutral Ara,[48] Xyl,[48] Glc,[49] and Gal[50] from the literature, recalculated at the B3LYP/6−311+G(d,p) level of theory. Hydrogen bond lengths are shown in angstroms.

TABLE 2: Anomeric Effect (kJ/mol) for Neutral Monosaccharides[a]

species	B3LYP	B3P86	MP2 (full)	species	B3LYP	B3P86	MP2 (full)
β-Ara	0.0	0.0	0.0	α-Glc	0.0	0.0	0.0
α-Ara	4.3	4.7	6.7	β-Glc	1.8	2.5	3.6
α-Xyl	0.0	0.0	0.0	α-Gal	0.2	0.0	0.0
β-Xyl	1.9	2.7	3.8	β-Gal	0.0	0.5	2.5

[a] Structures from literature[48−50] recalculated at the B3LYP/6−311+G(d,p) level with B3LYP, B3P86, and MP2(full) single point energies determined using a 6−311+G(2d,2p) basis set. All values include zero-point energy effects.

The anomeric effect of monosaccharides in the gas phase varies considerably from that in aqueous environments. The aqueous anomeric effect (i.e., the ratio of the different conformers in solution) is critical to our experiments because our electrospray source generates ionic species taken directly from the solution phase. Once in the gas phase, the monosaccharides cannot change anomericity, as this is a solvent-mediated process,[62] although some changes in this ratio may occur upon solvent desorption intrinsic to the electrospray process. To a first approximation, the relative abundance of the two anomeric forms in our gas-phase Na^+(α-L) and Na^+(β-L) experimental complexes should match that of the ligands under aqueous conditions. These ratios have been experimentally determined using NMR spectroscopy for each of the monosaccharides studied here[63,64] and are provided in Figure 3. For the pentoses, Ara and Xyl, the α to β ratio is 60:35.5% and 36.5:63%, respectively. For the hexoses, Glc and Gal, the α to β ratio is 38:62%.and 30:64%, respectively. Uncertainties in these values are cited at <3% in all cases.[63,64] An additional ring conformation is possible, a five-membered furanose ring form, but the abundance of this conformer is small (<6%)[63,64] and has therefore been ignored in the present study. Because the experimental abundance of both anomeric conformers of each monosaccharide is appreciable, we provide a comprehensive theoretical analysis for all eight sodiated structures here.

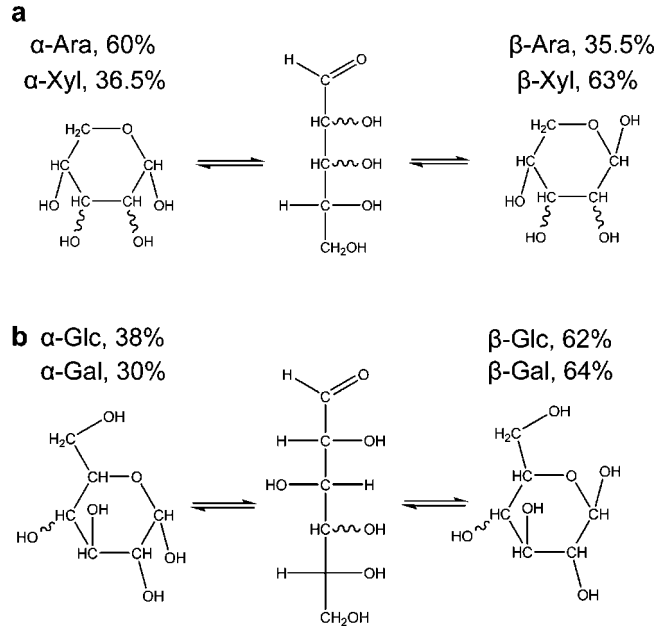

Figure 3. Relative abundances and structures of possible monosaccharide conformers in aqueous conditions as determined by NMR experiments for Ara, Xyl, Glc, and Gal.[63,64]

Complexes of these species with Na^+ were calculated as described above. The numbering scheme and ring-conformer nomenclature are provided in Figure 4.[25,65] A number of low-energy conformations for each complex were determined, and the five lowest energy conformers are provided in Figures 5 (α and β Ara), 6 (α and β Xyl), 7 (α and β Glc), and 8 (α and β Gal). Structures are named by their ring conformation (C for chair and B for boat with numbering described in Figure 4), their binding sites to the sodium cation (in brackets), and either by the total number of hydrogen bonds, H_T, or by the orientation of the hydrogen bonds, (Hx where x indicates the number of the oxygens covalently bound to the bridging hydrogen atom) when needed for distinction. Structural parameters and relative energies of the lowest energy conformations are provided in Tables 3 (pentose complexes) and 4 (hexose complexes).

For Ara, the low energy structures for the α and β forms have similar orientations. The GS structures determined by our DFT methods are [O2,O3] bidentate with $^1C_4$ ring conformations. Here the major structural difference between the two forms

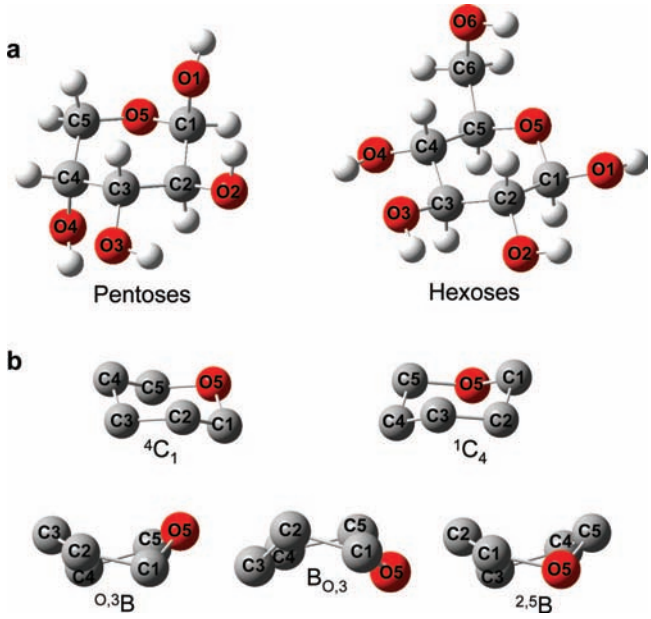

Figure 4. Numbering scheme (a) and ring conformations (b) for the monosaccharide complexes determined here.[25,65]

is the number of hydrogen bonds achieved, where the α anomer forms three and the β anomer forms four. The GS structure determined by our MP2(full) calculations for each form is tridentate, [O1,O4,O5] and [O1,O2,O5] for the α and β forms, respectively. Here the anomers also differ in their chair ring conformations, $^1C_4$ and $^4C_1$, respectively, and the number of hydrogen bonds achieved, four and one for the α and β anomers, respectively. The structure next highest in energy (5.0−5.4 and 8.4−10.7 kJ/mol for the α and β forms, respectively) are each $^1C_4$[O1,O2] bidentate and form three hydrogen bonds each. Lastly, each conformer can exist in low-energy boat ring conformations. For α-Ara, this results most favorably in [O1,O3,O4,O5] tetradentate binding orientations with a boat conformation of either $B_{O,3}$ or $^{2,5}B$ that lie 3.4−8.7 kJ/mol above the GS. These structures differ only in their B3P86 energies, Table 3. For β-Ara, the $^{2,5}B$ boat conformation results in tridentate [O3,O4,O5] binding similar to the comparable α-Ara structure but without the availability of the anomeric oxygen to participate in sodium cation binding. Further, the $^{O,3}B$ boat conformation of β-Ara most favorably achieves bidentate [O2,O3] binding. These structures lie 11.4−23.8 kJ/mol above the GS.

For Xyl, the low energy structures for the α and β forms differ slightly more than for the Ara system. Here the GS conformations are [O1,O2,O4,O5] tetradentate and [O2,O4,O5] tridentate for the α and β forms, respectively, each with $^1C_4$ ring orientations. The structure next highest in energy for α-Xyl lies 12.1−18.4 kJ/mol above the GS and has an [O2,O3] bidentate binding geometry with three hydrogen bonds. The β form prefers an [O1,O5] bidentate geometry with its anomeric oxygen. This orientation forms three hydrogen bonds and lies 24.8−30.1 kJ/mol above the GS. The two structures next highest in energy for α-Xyl are tridentate and bidentate structures, respectively, with chair ring conformations. They lie 12.2−25.1 kJ/mol above the GS. In contrast, each of the three structure next highest in energy for β-Xyl exist in boat ring conformations. Two tridentate [O1,O3,O5] $^{O,3}B$ geometries differ only in the orientation of the hydrogen bonds formed, where the H4 structure lies 2.8 −5.7 kJ/mol lower in energy than the H2 structure. The bidentate [O1,O2] structure for β-Xyl lies

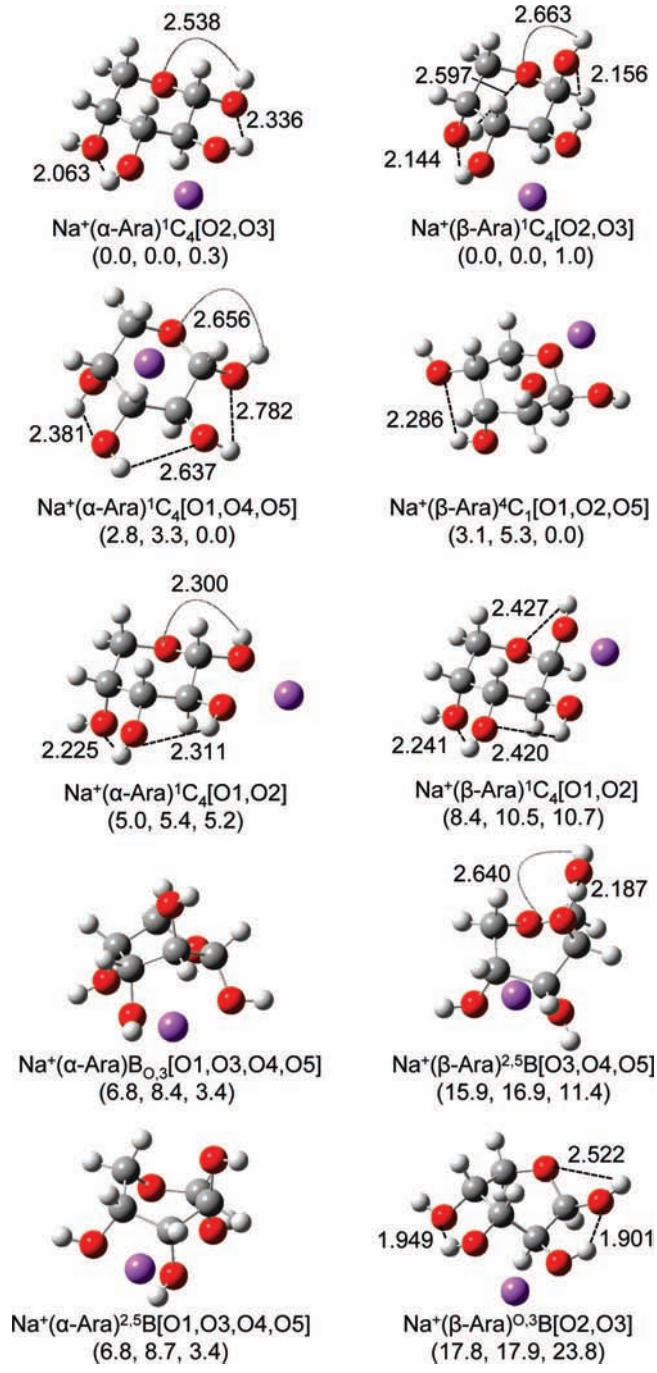

Figure 5. Ground state and low energy structures for sodium-bound α and β arabinose calculated at B3LYP/6−311+G(d,p) level. Hydrogen bond lengths are shown in Å. Energies (kJ/mol) from Table 3 relative to the ground state (top) are indicated at the B3LYP, B3P86, and MP2(full) levels of theory using a 6−311+G(2d,2p) basis set with geometries calculated at B3LYP/6−311+G(d,p) level.

31.0−40.3 kJ/mol above the GS. α-Xyl can also form a low-energy boat ring conformation with [O1,O4,O5] tridentate binding that lies 24.9−30.3 kJ/mol above the GS.

For Glc, the GS α and β complexes differ considerably. The α anomer exists in a chair ring conformation with an [O3,O4] bidentate binding geometry, and the β anomer exists in a boat ring conformation with an [O1,O3,O5,O6] tetradentate binding geometry, with four and two total hydrogen bonds, respectively. The structure next highest in energy for the α and β forms are similar, with $^4C_1$ ring conformations and [O2,O3] bidentate binding geometries, lying 8.6−9.0 and 3.4−10.7 kJ/mol above

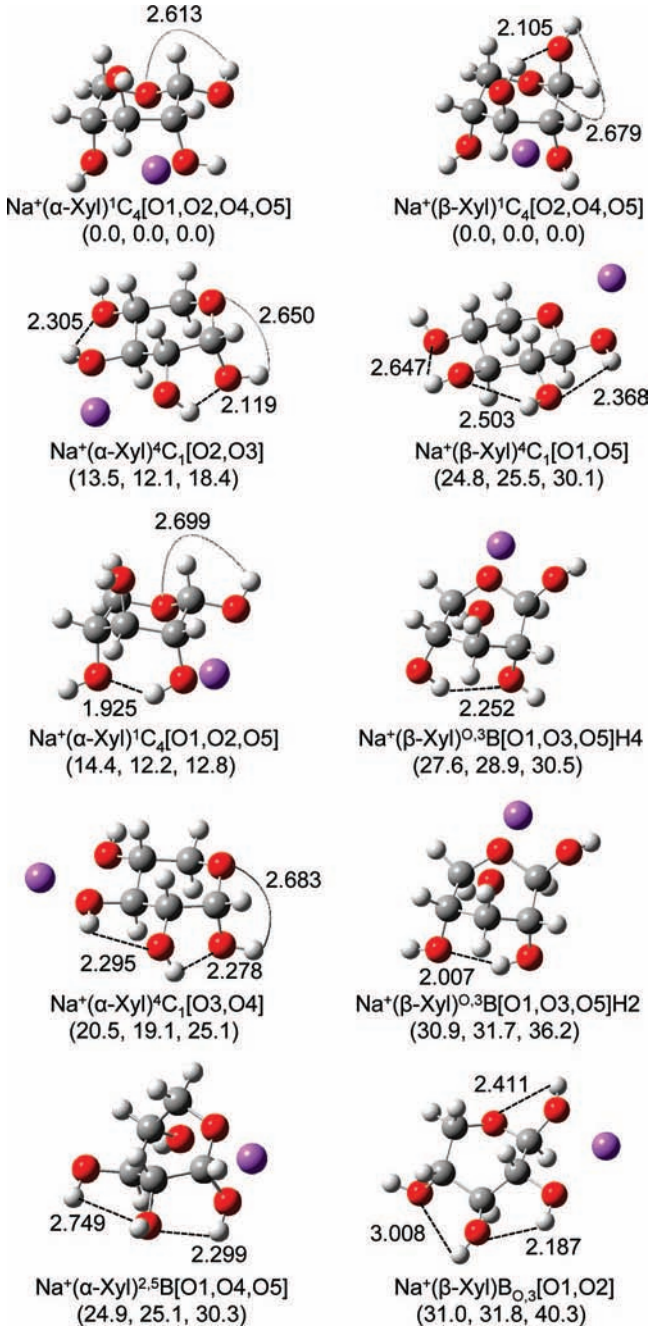

Figure 6. Ground state and low energy structures for sodium-bound α and β xylose calculated at B3LYP/6−311+G(d,p) level. Hydrogen bond lengths are shown in Å. Energies (kJ/mol) from Table 3 relative to the ground state (top) are indicated at the B3LYP, B3P86, and MP2(full) levels of theory using a 6−311+G(2d,2p) basis set with geometries calculated at B3LYP/6−311+G(d,p) level.

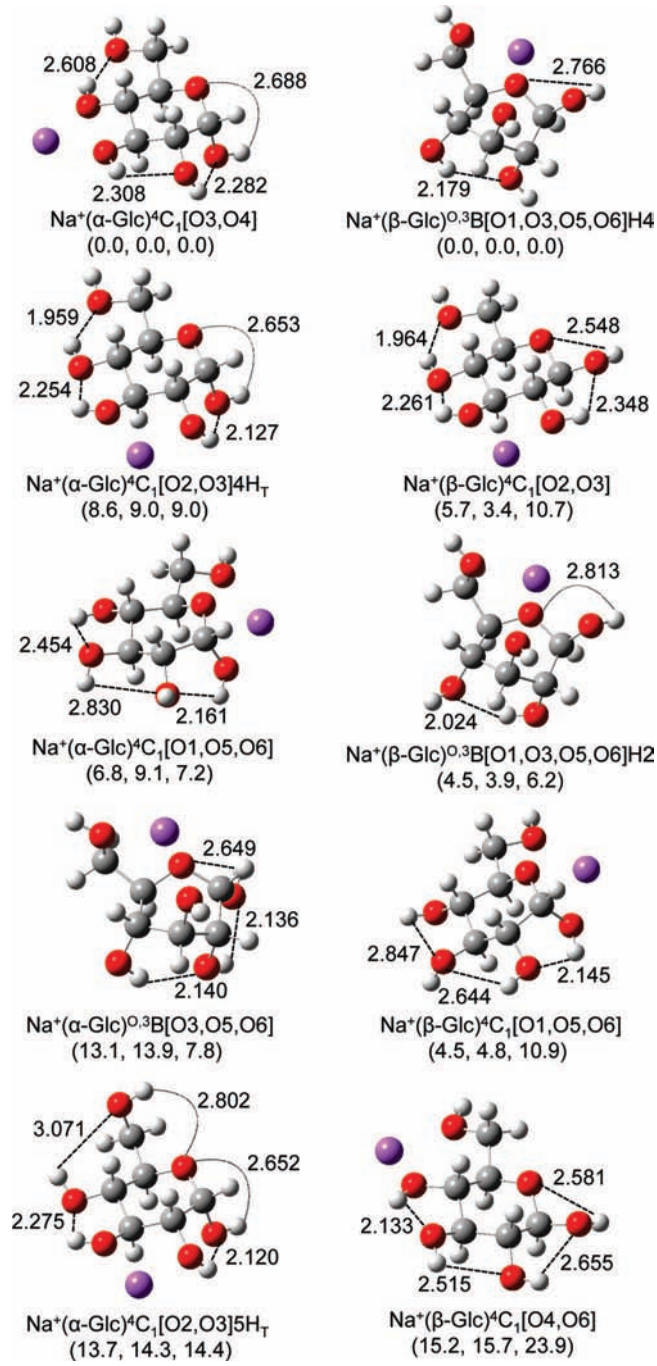

Figure 7. Ground state and low energy structures for sodium-bound α and β glucose calculated at B3LYP/6−311+G(d,p) level. Hydrogen bond lengths are shown in angstroms. Energies (kJ/mol) from Table 4 relative to the ground state (top) are indicated at the B3LYP, B3P86, and MP2(full) levels of theory using a 6−311+G(2d,2p) basis set with geometries calculated at B3LYP/6−311+G(d,p) level.

their GSs, respectively. The structure next highest in energy for the β-Glc complex is analogous to its GS and differs only in the orientation of hydrogen bonding, resulting in an energy difference of 3.9−6.2 kJ/mol. The final structures considered for the β complexes are each $^4C_1$ ring conformations and have tridentate [O1,O5,O6] and bidentate [O4,O6] binding geometries. α-Glc forms a [O1,O5,O6] tridentate structure similar to the β-Glc conformer that lies 6.8−9.1 kJ/mol above its GS. The lowest-energy boat conformation for α-Glc is analogous to the GS of Na^+(β-Glc) but can only achieve tridentate [O3,O5,O6] binding, unlike the tetradentate orientation of Na^+(β-Glc). This tridentate Na^+(α-Glc) structure lies 7.8−13.9 kJ/mol above its GS. Lastly, Na^+(α-Glc) can form an additional bidentate [O2,O3] geometry with five total hydrogen bonds (compared to four in the lower-energy [O2,O3] conformation). Although the total number of hydrogen bonds is greater in this structure, two are relatively long (2.802 and 3.071 Å) compared to the lower-energy structure that replaces these two long hydrogen bonds with one short one (1.959 Å).

For Gal, the α and β complexes form analogous low-energy structures. Each GS has a $^4C_1$ ring conformation and [O4,O5,O6] tridentate binding. The α and β structures next highest in energy have $^4C_1$ ring conformations and [O3,O4] bidentate binding. The α complex lies 3.8−8.3 kJ/mol above its GS, and the β

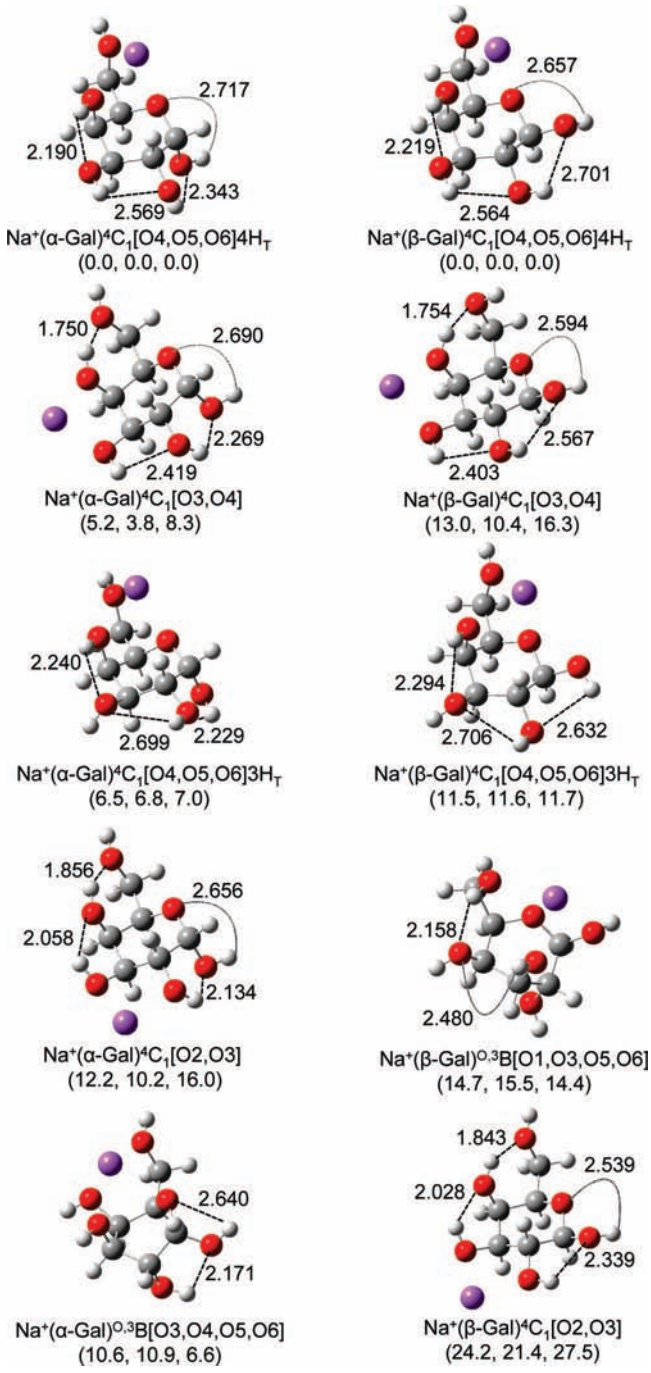

Figure 8. Ground state and low energy structures for sodium-bound α and β galactose calculated at B3LYP/6−311+G(d,p) level. Hydrogen bond lengths are shown in angstroms. Energies (kJ/mol) from Table 4 relative to the ground state (top) are indicated at the B3LYP, B3P86, and MP2(full) levels of theory using a 6−311+G(2d,2p) basis set with geometries calculated at B3LYP/6−311+G(d,p) level.

complex lies 10.4−16.3 kJ/mol above its GS. The third highest-energy structure for both the α and β forms is analogous to their GS conformations, differing only in the orientation and number of total hydrogen bonds formed (three compared to four), with energy differences of 6.5−7.0 kJ/mol and 11.5−11.7 kJ/mol for the α and β forms, respectively. The fourth structure for β-Gal exists in a boat ring conformation with [O1,O3,O5,O6] tetradentate binding, lying 14.4−15.5 kJ/mol above its GS. An analogous α complex cannot be formed, as the anomeric oxygen participates in the binding here. A low-energy $^4C_1$[O2,O3] geometry is exhibited by both anomeric forms and lies 10.2−16.0 kJ/mol above the GS for the α anomer and 21.4−27.5 kJ/mol above the GS for the β anomer. Lastly, the α anomer forms a low-energy boat conformation with [O3,O4,O5,O6] tetradentate binding, which lies 6.6−10.9 kJ/mol above the GS.

Discussion

Sensitivity to Anomeric Identity: What is Being Measured? The sodium cation affinities measured experimentally in this study for each Na^+(L) system correspond to a mixture of two anomeric forms, as discussed above. Clearly, this complicates the analysis of the systems under study and necessitates further investigation as to what our measured thresholds correspond to. A comparison of our theoretically determined bond energies for the anomeric forms of each system, Table 5, gives an anomeric BDE effect of 3−5 kJ/mol for Na^+(Ara), 10−13 kJ/mol for Na^+(Xyl), 0−9 kJ/mol for Na^+(Glc), and 6−8 kJ/mol for Na^+(Gal). Given these small differences in binding energies between anomers (<13 kJ/mol), our experimentally measured thresholds should correspond to eq 4,

$$D_0(Na^+ - L) = D_0(Na^+ - \alpha L) \times (\%\ \alpha\ L) + D_0(Na^+ - \beta L) \times (\%\beta L) \quad (4)$$

an average of the anomeric forms weighted by the experimental aqueous distribution assumed to correspond to each conformer, as detailed in Figure 3. It is important to note that these experimental abundances correspond to aqueous conditions. Our stock solutions are made in purely aqueous solvent and further diluted into a 50:50 by volume MeOH:H_2O solution. The potential variation in anomeric ratio resulting from this addition is taken into account in our experimental uncertainties, especially considering that the more volatile methanol molecules likely evaporate preferentially to the water molecules during the electrospray ionization process. Thus, the electrospray droplets should become more aqueous-like in their anomeric distribution as evaporation during the electrospray process proceeds.

Using the theoretical values for $\Delta D_0(Na^+$-L), i.e.,

$$\Delta D_0(Na^+ - L) = D_0(Na^+ - \alpha L) - D_0(Na^+ - \beta L) \quad (5)$$

Equation 4 can be rearranged to

$$D_0(Na^+ - \alpha L) = D_0(Na^+ - L)_{exp} + \%\beta L \times \Delta D_0(Na^+ - L) \quad (6)$$

and

$$D_0(Na^+ - \beta L) = D_0(Na^+ - L)_{exp} + \%\alpha L \times \Delta D_0(Na^+ - L) \quad (7)$$

to determine the BDEs for each anomeric form.

To explicitly test the validity of these assumptions, we calculated the additive contributions of each anomeric conformer with the adjusted threshold energies calculated according to eqs 6 and 7 in their assumed experimental distribution for the system with the largest $\Delta D_0(Na^+$-L) value, Na^+(Xyl). Using the theoretically determined value of $\Delta D_0(Na^+$-Xyl), 11 kJ/mol, the reproduction of the data is comparable to that shown in Figure 1b. We also examined how the reproduction of the data changed as the value of $\Delta D_0(Na^+$-L) increased, including values of 13, 15, 17, 20, 24, 28, and 30 kJ/mol. For $\Delta D_0(Na^+$-L) < 20 kJ/mol, the data continue to be reproduced accurately within the experimental uncertainties of the cross-sections. For $\Delta D_0(Na^+$-L) > 20 kJ/mol, the data are no longer reproduced with fidelity,

TABLE 3: Bond Distances (Å) and Relative Energies (kJ/mol) for Low-Energy Structures of Sodiated Pentoses[a]

species	$r(Na^+$-Oa)	$r(Na^+$-Ob)	$r(Na^+$-Oc)	$r(Na^+$-Od)	B3LYP	B3P86	MP2(full)
Na^+(α-Ara)$^1C_4$[O2,O3]	2.268	2.269			0.0	0.0	0.3
$^1C_4$[O1,O4,O5]	3.007	2.335	2.284		2.8	3.3	0.0
$^1C_4$[O1,O2]	2.275	2.250			5.0	5.4	5.2
$B_{O,3}$[O1,O3,O4,O5]	2.485	2.349	2.401	2.402	6.8	8.4	3.4
^{2,5}B[O1,O3,O4,O5]	2.428	2.346	2.468	2.406	6.8	8.7	3.4
Na^+(β-Ara)$^1C_4$[O2,O3]	2.295	2.275			0.0	0.0	1.0
$^4C_1$[O1,O2,O5]	2.347	2.307	2.389		3.1	5.3	0.0
$^1C_4$[O1,O2]	2.237	2.239			8.4	10.5	10.7
^{2,5}B[O3,O4,O5]	2.290	2.325	2.412		15.9	16.9	11.4
^{O,3}B[O2,O3]	2.256	2.260			17.8	17.9	23.8
Na^+(α-Xyl) $^1C_4$[O1,O2,O4,O5]	3.171	2.331	2.313	2.357	0.0	0.0	0.0
$^4C_1$[O2,O3]	2.275	2.262			13.5	12.1	18.4
$^1C_4$[O1,O2,O5]	2.330	2.312	2.445		14.4	12.2	12.8
$^4C_1$[O3,O4]	2.236	2.282			20.5	19.1	25.1
^{2,5}B[O1,O4,O5]	2.276	2.317	2.399		24.9	25.1	30.3
Na^+(β-Xyl) $^1C_4$[O2,O4,O5]	2.303	2.281	2.410		0.0	0.0	0.0
$^4C_1$[O1,O5]	2.246	2.295			24.8	25.5	30.1
^{O,3}B[O1,O3,O5]H4	2.343	2.286	2.349		27.6	28.9	30.5
^{O,3}B[O1,O3,O5]H2	2.323	2.305	2.345		30.9	31.7	36.2
$B_{O,3}$[O1,O2]	2.295	2.267			31.0	31.8	40.3

[a] Structures calculated at B3LYP/6−311+G(d,p) level of theory. Single point energies determined at B3LYP, B3P86, MP2(full)/6−311+G(2d,2p) //B3LYP/6−311+G(d,p).

TABLE 4: Bond Distances (Å) and Relative Energies (kJ/mol) for Low-energy Structures of Sodiated Hexoses[a]

Species	r(Na^+-Oa)	R(Na^+-Ob)	r(Na^+-Oc)	r(Na^+-Od)	B3LYP	B3P86	MP2(full)
Na^+(α-Glc)$^4C_1$[O3,O4]	2.250	2.236			0.0	0.0	0.0
$^4C_1$[O2,O3]$4H_T$	2.283	2.249			8.6	9.0	9.0
$^4C_1$[O1,O5,O6]	2.388	2.401	2.300		6.8	9.1	7.2
^{O,3}B[O3,O5,O6]	2.313	2.340	2.270		13.1	13.9	7.8
$^4C_1$[O2,O3]$5H_T$	2.281	2.254			13.7	14.3	14.4
Na^+(β-Glc) ^{O,3}B[O1,O3,O5,O6]H4	2.635	2.326	2.293	2.358	0.0	0.0	0.0
$^4C_1$[O2,O3]	2.266	2.246			5.7	3.4	10.7
^{O,3}B[O1,O3,O5,O6]H2	2.537	2.347	2.287	2.377	4.5	3.9	6.2
$^4C_1$[O1,O5,O6]	2.377	2.399	2.305		4.5	4.8	10.9
$^4C_1$[O4,O6]	2.205	2.231			15.2	15.7	23.9
Na^+(α-Gal)$^4C_1$[O4,O5,O6]$4H_T$	2.271	2.435	2.231		0.0	0.0	0.0
$^4C_1$[O3,O4]	2.258	2.218			5.2	3.8	8.3
$^4C_1$[O4,O5,O6]$3H_T$	2.295	2.392	2.234		6.5	6.8	7.0
$^4C_1$[O2,O3]	2.280	2.269			12.2	10.2	16.0
^{O,3}B[O3,O4,O5,O6]	2.344	2.384	2.499	2.275	10.6	10.9	6.6
Na^+(β-Gal)$^4C_1$[O4,O5,O6]$4H_T$	2.309	2.365	2.259		0.0	0.0	0.0
$^4C_1$[O3,O4]	2.259	2.215			13.0	10.4	16.3
$^4C_1$[O4,O5,O6]$3H_T$	2.372	2.315	2.279		11.5	11.6	11.7
^{O,3}B[O1,O3,O5,O6]	2.485	2.381	2.302	2.388	14.7	15.5	14.4
$^4C_1$[O2,O3]	2.268	2.260			24.2	21.4	27.5

[a] Structures calculated at B3LYP/6−311+G(d,p) level of theory. Single point energies determined at B3LYP, B3P86, MP2(full)/6−311+G(2d,2p) //B3LYP/6−311+G(d,p).

TABLE 5: Experimental, Theoretical, and Literature Sodium Affinities at 0 K (kJ/mol)

complex	experiment[a]	adjusted values[b]	B3LYP[c,d]	B3P86[c,d]	MP2(full)[c]	MP2(full,cp)[c,d]	literature[e]
Na^+(α-Ara)	171 (6)	172 (6)	172	167	173	161	168 (7)
Na^+(β-Ara)		169 (6)	169	164	169	156	
Na^+(α-Xyl)	181 (6)	188 (6)	185	178	191	177	169 (7)
Na^+(β-Xyl)		177 (6)	172	167	180	167	
Na^+(α-Glc)	181 (7)	184 (8)	190	185	190	180	172 (7)
Na^+(β-Glc)		179 (8)	183	176	190	175	
Na^+(α-Gal)	203 (7)	198 (7)	197	190	200	186	175 (7)
Na^+(β-Gal)		205 (7)	203	196	208	193	
MAD[f]			3 (2)	6 (3)	4 (3)	10 (4)	

[a] Present experimental values from Table 1. Uncertainties in parentheses. [b] Values determined using eqs 6 and 7. [c] Calculations performed at the stated level of theory using a 6−311+G(2d,2p) basis set with geometries calculated at B3LYP/6−311+G(d,p) level. [d] Counterpoise corrected. [e] Kinetic method results from Wesdemiotis and co-workers. [f] Mean absolute deviation from present experimental values.

with pronounced deviations primarily in the threshold region. We therefore conclude that our assumptions are valid for $\Delta D_0(Na^+$-L) values up to 20 kJ/mol, well within the range needed in the current study for all four saccharides. Thus, we determine the sodium cation BDEs for each anomeric form of Ara, Xyl, Glc, and Gal, provided in Table 5, where the %αL

TABLE 6: Enthalpies and Free Energies of Sodium Binding at 0 and 298 K (kJ/mol)[a]

complex	ΔH_0[b]	$\Delta H_{298} - \Delta H_0$[c]	ΔH_{298}	$T\Delta S_{298}$[c]	ΔG_{298}
Na^+(α-Ara)	172 (6)	2.1 (0.3)	174 (6)	33.8 (4.0)	140 (7)
Na^+(β-Ara)	169 (6)	1.8 (0.2)	171 (6)	33.0 (3.9)	138 (7)
Na^+(α-Xyl)	188 (6)	1.4 (0.2)	189 (6)	33.7 (4.0)	156 (7)
Na^+(β-Xyl)	177 (6)	2.3 (0.3)	179 (6)	36.5 (4.3)	143 (7)
Na^+(α-Glc)	184 (8)	2.8 (0.3)	187 (8)	35.5 (3.1)	151 (9)
Na^+(β-Glc)	179 (8)	1.6 (0.1)	181 (8)	35.2 (3.1)	145 (9)
Na^+(α-Gal)	198 (7)	2.1 (0.2)	200 (7)	36.4 (3.7)	164 (8)
Na^+(β-Gal)	205 (7)	2.3 (0.2)	207 (7)	35.9 (3.6)	171 (8)

[a] Uncertainties in parentheses. [b] Experimental values from Table 5. [c] Calculated using standard formulas and molecular constants calculated at the B3LYP/6−311+G(d,p) level.

and %βL values used in eqs 6 and 7 exclude minor abundances of the furanose forms of the pentoses, as noted previously. Uncertainties in these anomeric-specific bond energies include the experimental uncertainties in the threshold energies listed in Table 1, the theoretical uncertainties in $\Delta D_0(Na^+\text{-L})$, and a conservative uncertainty of 10% in the anomeric distributions that account for the uncertainty in the NMR spectroscopy experiments,[63,64] the exclusion of the minor furanose forms, and the possibility that these ratios likely vary slightly upon binding to Na^+ and during the evaporation process when introduced into the gas-phase, as noted above.

Conversion from 0 to 298 K and Excited Conformers. Conversion from 0 K bond energies to 298 K bond enthalpies and free energies is accomplished using the rigid rotor/harmonic oscillator approximation with rotational constants and vibrational frequencies calculated at the B3LYP/6−311+G(d,p) level. These ΔH_{298} and ΔG_{298} values along with the conversion factors and 0 K enthalpies measured here are reported in Table 6. The uncertainties listed are determined by scaling most of the vibrational frequencies by ±10% along with 2-fold variations in the metal−ligand frequencies. We also calculated the ΔG_{298} values for the second lowest energy structure of all eight Na^+(L) systems. In general, the relative ΔG_{298} excitation energies are comparable to the analogous differences in the ΔH_0 values, Tables 3 and 4.

The theoretical BDEs discussed below are all calculated for the most stable Na^+(L) conformations. For some of the systems, it is possible that the complexes formed experimentally in the source region at thermal energies may consist of multiple low-energy conformers. Although no obvious evidence for multiple conformers is found experimentally, the sensitivity of TCID experiments to low energy species is not particularly acute. Using the ΔG_{298} values to calculate an equilibrium population of conformers shows that the calculated GS structures for most Na^+(L) systems should be dominant in the room temperature ion sources. Excited conformers for the Na^+(Xyl) and Na^+(β-Gal) systems are calculated to comprise <1% of the total population, and excited conformers for the Na^+(α-Glc) system are calculated to comprise ~3% of the total population. In contrast, excited conformers of the Na^+(Ara) system are calculated to comprise 11−47% of the total population and 1−20% for the Na^+(β-Glc) and Na^+(α-Gal) systems (depending on the level of theory). To investigate the effect of having a different conformer populating the Na^+(Ara), Na^+(β-Glc), and Na^+(α-Gal) reactant ions, we reanalyzed the data using the molecular parameters of the second lowest energy structure for these systems. The threshold energies change by less than 1 kJ/mol in all cases, similar to the difference obtained between the anomeric forms, and this effect is included in the experimental uncertainties listed in the tables. Thus, even if there are multiple conformers present in the reactant ion beams, this does not affect the thermochemistry derived within the stated experimental uncertainties.

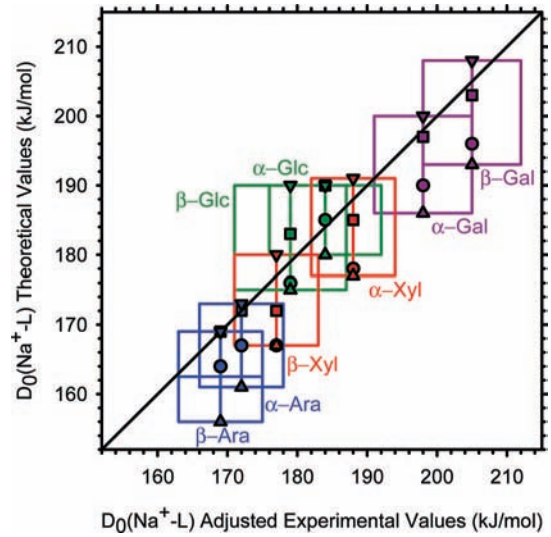

Figure 9. Adjusted experimental and theoretical bond energies (kJ/mol) of sodium cations bound to the eight monosaccharide anomers. Theoretical values include those calculated at the B3LYP (squares), B3P86 (circles), MP2(full) (downward triangles), and MP2(full,cp) (upward triangles) levels. All values from Table 5.

Comparison of Experimental, Theoretical, and Literature Values. The sodium cation affinities for the eight molecules examined in this study as measured using TCID with the guided ion beam mass spectrometer and calculated here are summarized in Table 5 and Figure 9. The calculated binding energies refer to the ground-state conformations of each system, and thus correspond to different conformations for the Na^+(Ara) systems, but none of the other saccharides. The agreement between theory and experiment for the monosaccharides studied here is extremely good. Theoretical calculations span the range of our experimentally determined values in all cases. Of this range, the values determined theoretically at the MP2(full) level including counterpoise corrections fall consistently below experimental values with a mean absolute deviation (MAD) of 10 ± 4 kJ/mol. By comparison, MP2(full) calculations excluding counterpoise give much better agreement and are systematically high, with a MAD of 4 ± 3 kJ/mol. Overall, the use of BSSE corrections appears to overcorrect in these systems. Values calculated at the B3LYP level yield values that are in excellent agreement with experiment, with a MAD of only 3 ± 2 kJ/mol (and an average deviation of 0.1 ± 3.6 kJ/mol). Lastly, values calculated at the B3P86 level have a MAD of 6 ± 3 kJ/mol and are generally too low. All of these variations are comparable to the average experimental uncertainty of 6−8 kJ/mol.

Sodium cation binding affinities for the four amino acids were determined previously by Wesdemiotis and co-workers[25] with tandem mass spectrometry using Cook's kinetic method[26,27] relative to reference bases with known Na^+ affinities. Their values at 298 K are Na^+(Ara) = 170, Na^+(Xyl) = 171, Na^+(Glc) = 174 and Na^+(Gal) = 177 kJ/mol, all with relative uncertainties of ±1 kJ/mol and absolute uncertainties of ±7 kJ/mol. When adjusted to 0 K using the data in Table 6 for comparison with our results, the BDEs become 168, 169, 172, and 175 ± 7, respectively. These experimental trends match ours before anomericity correction, i.e., Ara < Xyl < Glc < Gal; however, only the Na^+(Ara) BDE agrees reasonably well with our

experimentally determined values before adjustment for anomericity. The BDEs for Na^+(Xyl) and Na^+(Glc) do fall within the combined experimental errors, but for Na^+(Gal), the gap between the experimental values is 28 kJ/mol, well outside of the experimental uncertainties. Furthermore, the span of values in the kinetic method results is only 7 kJ/mol compared to our span of 32 kJ/mol, whereas theory predicts ranges of 34 (B3LYP), 32 (B3P86), and 37 (MP2) kJ/mol, clearly inconsistent with the kinetic method results. It should be pointed out that their experimental samples were prepared in thioglycerol solutions, and the abundance of the different anomeric forms in their experiments was never assessed. It is unlikely that the difference in solvent conditions can account for the large deviation in values between experimental results, and the difference in the binding of anomeric forms is not large enough to do so either. Notably, kinetic methods experiments are limited by the choice of reference base used and often provide too small a range of values among comparable ligands; see Heaton et al.[66] for a recent example.

Additionally, Wesdemiotis and co-workers[25] supplemented their experimental results with theoretical calculations performed at the HF/6−31G* level with single point energies obtained at the B3LYP/6−311+G(2d,2p) level of theory, and BSSE corrections at the same level. They assessed structures of both α and β anomeric forms of each sodiated monosaccharide complex but mention that their theoretical results are used only to rationalize experimental trends and are not quantifiable with their experimental results. They find GS structures for each complex that involve the maximum coordination number with the sodium cation. For the Na^+(Xyl) and Na^+(β-Glc) systems, their GSs are identical to ours, as these complexes happen to involve high coordination numbers. In contrast, the GS structures they determine for the Na^+(Ara), Na^+(α-Glc), and Na^+(Gal) systems do not match the ground-state conformations determined here. We find that their Na^+(α-Ara)^{2,5}B[O1,O3,O4,O5] and Na^+(β-Ara)^{2,5}B[O3,O4,O5] conformations lie 3.4−8.7 and 11.4−16.9 kJ/mol above our GS conformers, respectively. Additionally, we find that their Na^+(α-Glc)^{O,3}B[O3,O5,O6], Na^+(α-Gal)^{O,3}B[O3,O4,O5,O6], and Na^+(β-Gal)^{O,3}B[O1,O3,O5,O6] structures lie 7.8−13.9, 6.6−10.9, and 14.4−15.5 kJ/mol above our GSs, respectively.

Qualitative Trends. The monosaccharides examined in this study comprise both pentoses (Ara and Xyl) and hexoses (Glc and Gal), each existing in α and β anomeric forms in solution. The experimental sodium binding affinities determined from our electrospray solution samples follow the trend pentoses < hexoses, and more specifically Ara < Xyl < Glc < Gal. Yet consideration of the anomeric BDE effect, determined theoretically here, allows eqs 6 and 7 to be used to provide sodium binding affinities for all eight anomers, which follow the trend β-Ara < α-Ara < β-Xyl < β-Glc < α-Glc < α-Xyl < α-Gal < β-Gal, Table 5 and Figure 9. The smallest sodium affinities are found for the Ara systems. Here the GS ring structures are all chair conformations, which bind bidentate to the sodium cation in the GS determined by our DFT methods, [O2,O3], and tridentate in the GS determined by our MP2(full) calculations [O1,O4,O5] and [O1,O2,O5] for the α and β forms, respectively. For the Xyl systems, which bind sodium more tightly than the Ara systems, both the α and β GSs also have chair ring conformations, but the α- conformer binds tetradentate with its anomeric oxygen, [O1,O2,O4,O5], where the β-conformer can only bind tridentate, [O2,O4,O5]. This decreases the sodium cation affinity of the β-conformer of Xyl by 11 kJ/mol relative to the α-conformer. Bridged between the anomers of Xyl in sodium binding affinity are the Glc systems. α-Glc binds more tightly than β-Glc, even though the GS of Na^+(β-Glc) is tetradentate [O1,O3,O5,O6] and the GS of Na^+(α-Glc) is bidentate [O3,O4]. This difference likely lies in steric constraints, as the β conformer has a boat ring conformation in its GS, whereas the α conformer has a much more stable chair ring conformation. Calculations of these conformers in the absence of the sodium cation indicate that the boat β conformation of Glc lies 67.1, 71.2, and 67.5 kJ/mol (ZPEs not included) higher in energy than the chair α conformation at the B3LYP, B3P86, and MP2(full)/6−311+G(2d,2p) levels of theory. The largest sodium cation affinity is found for the Gal systems, which achieve highly stabilized tridentate [O4,O5,O6] binding with chair ring conformations in their GSs.

We find that a number of factors affect the stability of sodium cation binding to the monosaccharides studied here. Although high-coordination multidentate Na^+ binding can be highly stabilizing, as in the Gal and Xyl systems, the total energy can be reduced when high-coordination binding can only be achieved with a less sterically and energetically favored boat ring conformation. Additionally, the number of hydrogen bonds achieved can stabilize the sodiated monosaccharide structures, but when additional hydrogen bonding results in larger hydrogen bond lengths, a structure with fewer, shorter hydrogen bonds may be preferred.

Conclusion

The kinetic energy dependence of the collision-induced dissociation of Na^+(L), L = D-arabinose, xylose, glucose, and galactose, with Xe are examined in a guided ion beam mass spectrometer. Thresholds at 0 K for the Na^+-affinity of the monosaccharides are determined after consideration of the effects of reactant internal energy, multiple collisions with Xe, and lifetime effects using a phase space limit transition state model.[43] The experimental binding energies correspond to a mixture of the α and β anomeric forms for each system and are corrected using the theoretically determined anomeric sodium BDE effect to produce thresholds for α-Ara, β-Ara, α-Xyl, β-Xyl, α-Glc, β-Glc, α-Gal, and β-Gal. The binding energies determined are in excellent agreement with quantum chemical calculations using the B3LYP/6−311+G(2d,2p)//B3LYP/6−311+G(d,p) level of theory. Values reported here constitute the first direct measurements of these sodium cation binding affinities to these saccharides and, in combination with theory, values for all eight ligands are provided.

The experimental results supported by theoretical calculations permit a systematic evaluation of the binding motifs of each Na^+(L) complex, thereby allowing a dissection of binding trends among the ligands studied here. For each Na^+(L) complex, it is clear that the best binding motif is a multidentate binding association with the sterically favored chair ring conformation; however, when this cannot be achieved, the binding energy is reduced by either less coordinated binding or less sterically favored ring conformations. The systematic trends determined from our electrospray solutions are qualitatively consistent with the trends found in the available literature values,[25] but quantitative agreement is achieved only for Na^+(Ara). In addition, the anomeric correction allows a more complete assessment of the trends in binding for all anomeric forms of the monosaccharides studied here, i.e. β-Ara < α-Ara < β-Xyl < β-Glc < α-Glc < α-Xyl < α-Gal < β-Gal.

Acknowledgment. This work is supported by the National Science Foundation, Grant CHE-0748790. A grant of computer

time from the Center for High Performance Computing at the University of Utah is gratefully acknowledged.

References and Notes

(1) Moran, L. A.; Scrimgeour, K. G.; Horton, H. R.; Ochs, R. S.; Rawn, J. D. *Biochemistry*, 2nd ed.; Neil Patterson Publishers/Prentice-Hall Inc.: Englewood Cliffs, NJ, 1994.

(2) Pigman, W.; Horton, D. *The Carbohydrates: Chemistry and Biochemistry*; Academic Press: New York, 1972.

(3) Armentrout, P. B.; Rodgers, M. T. *J. Phys. Chem. A* **2000**, *104*, 2238.

(4) Rodgers, M. T.; Armentrout, P. B. *Mass Spectrom. Rev.* **2000**, *19*, 215.

(5) Rodgers, M. T.; Armentrout, P. B. *J. Phys. Chem. A* **1999**, *103*, 4955.

(6) Amicangelo, J. C.; Armentrout, P. B. *J. Phys. Chem. A* **2000**, *104*, 11420.

(7) More, M. B.; Ray, D.; Armentrout, P. B. *J. Am. Chem. Soc.* **1999**, *121*, 417.

(8) Fujii, T. *Mass Spectrom. Rev.* **2000**, *19*, 111.

(9) Hoyau, S.; Norrman, K.; McMahon, T. B.; Ohanessian, G. *J. Am. Chem. Soc.* **1999**, *121*, 8864.

(10) McMahon, T. B.; Ohanessian, G. *Chem. Eur. J.* **2000**, *6*, 2931.

(11) Rodgers, M. T. *J. Phys. Chem. A* **2001**, *105*, 8145.

(12) Rodgers, M. T. *J. Phys. Chem. A* **2001**, *105*, 2374.

(13) Bojesen, G.; Breindahl, T.; Andersen, U. N. *Org. Mass Spectrom.* **2005**, *28*, 1448.

(14) Kish, M. M.; Ohanessian, G.; Wesdemiotis, C. *Int. J. Mass Spectrom.* **2003**, *227*, 509.

(15) Rodgers, M. T.; Armentrout, P. B. *Acc. Chem. Res.* **2004**, *37*, 989.

(16) Harvey, D. J.; Martin, R. L.; Jackson, K. A.; Sutton, C. W. *Rapid Commun. Mass Spectrom.* **2004**, *18*, 2997.

(17) Carlesso, V.; Afonso, C.; Fournier, F.; Tabet, J. C. *Int. J. Mass Spectrom.* **2002**, *219*, 559.

(18) Harvey, D. J. *J. Mass Spectrom.* **2000**, *35*, 1178.

(19) Harvey, D. J.; Rudd, P. M.; Batemen, R. H.; Bordoli, R. S.; Howes, K.; Hoyes, J. B.; Vickers, R. G. *Org. Mass Spectrom.* **1994**, *29*, 753.

(20) Takegawa, Y.; Deguchi, K.; Nakagawa, H.; Nishimura, S. *Anal. Chem.* **2005**, *77*, 6062.

(21) Harvey, D. J. *J. Mass Spectrom.* **2005**, *40*, 642.

(22) Harvey, D. J. *J. Am. Soc. Mass. Spectrom.* **2005**, *16*, 622.

(23) Yamagaki, T.; Suzuki, H.; Tachibana, K. *J. Mass Spectrom.* **2006**, *41*, 454.

(24) Fang, T. T.; Bendiak, B. *J. Am. Chem. Soc.* **2007**, *129*, 9721.

(25) Cerda, B. A.; Wesdemiotis, C. *Int. J. Mass Spectrom.* **1999**, *189*, 189.

(26) Cooks, R. G.; Patrick, J. S.; Kotiaho, T.; McLuckey, S. A. *Mass Spectrom. Rev.* **1994**, *13*, 287.

(27) Cooks, R. G.; Wong, P. S. H. *Acc. Chem. Res.* **1998**, *31*, 379.

(28) Ervin, K. M.; Armentrout, P. B. *J. Chem. Phys.* **1985**, *83*, 166.

(29) Muntean, F.; Armentrout, P. B. *J. Chem. Phys.* **2001**, *115*, 1213.

(30) Moision, R. M.; Armentrout, P. B. *J. Am. Soc. Mass Spectrom.* **2007**, *18*, 1124.

(31) Kim, T.; Tolmachev, A. V.; Harkewicz, R.; Prior, D. C.; Anderson, G.; Udseth, H. R.; Smith, R. D. *Anal. Chem.* **2000**, *72*, 2247.

(32) Ye, S. J.; Armentrout, P. B. *J. Phys. Chem. A* **2008**, *112*, 3587.

(33) Teloy, E.; Gerlich, D. *Chem. Phys.* **1974**, *4*, 417.

(34) Gerlich, D. *Adv. Chem. Phys.* **1992**, *82*, 1.

(35) Aristov, N.; Armentrout, P. B. *J. Phys. Chem.* **1986**, *90*, 5135.

(36) Dalleska, N. F.; Honma, K.; Sunderlin, L. S.; Armentrout, P. B. *J. Am. Chem. Soc.* **1994**, *116*, 3519.

(37) Daly, N. R. *Rev. Sci. Instrum.* **1960**, *31*, 264.

(38) Beyer, T. S.; Swinehart, D. F. *Commun. ACM* **1973**, *16*, 379.

(39) Stein, S. E.; Rabinovitch, B. S. *J. Chem. Phys.* **1973**, *58*, 2438.

(40) Stein, S. E.; Rabinovitch, B. S. *Chem. Phys. Lett.* **1977**, *49*, 183.

(41) Gilbert, R. G.; Smith, S. C. *Theory of Unimolecular and Recombination Reactions*; Blackwell Scientific: London, 1990.

(42) Robinson, P. J.; Holbrook, K. A. Unimolecular Reactions; Wiley Interscience: New York, 1972.

(43) Rodgers, M. T.; Ervin, K. M.; Armentrout, P. B. *J. Chem. Phys.* **1997**, *106*, 4499.

(44) Rodgers, M. T.; Armentrout, P. B. *J. Chem. Phys.* **1998**, *109*, 1787.

(45) Hales, D. A.; Lian, L.; Armentrout, P. B. *Int. J. Mass Spectrom. Ion Processes* **1990**, *102*, 269.

(46) More, M. B.; Ray, D.; Armentrout, P. B. *J. Phys. Chem. A* **1997**, *101*, 7007.

(47) Armentrout, P. B.; Simons, J. *J. Am. Chem. Soc.* **1992**, *114*, 8627.

(48) Guler, L. P.; Yu, Y.-Q.; Kenttamaa, H. I. *J. Phys. Chem. A* **2002**, *106*, 6754.

(49) Barrows, S. E.; Storer, J. W.; Cramer, C. J.; French, A. D.; Truhlar, D. G. *J. Comput. Chem.* **1997**, *19*, 1111.

(50) Rahal-Sekkal, M.; Sekkal, N.; Kleb, D. C.; Bleckmann, P. *J. Comput. Chem.* **2002**, *24*, 806.

(51) Moision, R. M.; Armentrout, P. B. *J. Phys. Chem. A* **2002**, *106*, 10350.

(52) Pearlman, D. A.; Case, D. A.; Caldwell, J. W.; Ross, W. R.; Cheatham, T. E.; DeBolt, S.; Ferguson, D.; Seibel, G.; Kollman, P. *Comput. Phys. Commun.* **1995**, *91*, 1.

(53) Bylaska, E. J.; de Jong, W. A.; Kowalski, K.; Straatsma, T. P.; Valiev, M.; Wang, D. ; Aprà, E.; Windus, T. L.; Hirata, S.; Hackler, M. T.; Zhao, Y.; Fan, P.-D.; Harrison, R. J.; Dupuis, M.; Smith, D. M. A.; Nieplocha, J. ; Tipparaju, V.; Krishnan, M.; Auer, A. A.; Nooijen, M.; Brown, E.; Cisneros, G.; Fann, G. I. ; Früchtl, H.; Garza, J.; Hirao, K.; Kendall, R.; Nichols, J. A.; Tsemekhman, K.; Wolinski, K. ; Anchell, J. ; Bernholdt, D.; Borowski, P.; Clark, T.; Clerc, D.; Dachsel, H.; Deegan, M.; Dyall, K.; Elwood, D.; Glendening, E.; Gutowski, M.; Hess, A.; Jaffe, J.; Johnson, B.; Ju, J.; Kobayashi, R.; Kutteh, R.; Lin, Z.; Littlefield, R.; Long, X.; Meng, B.; Nakajima, T.; Niu, S.; Pollack, L.; Rosing, M.; Sandrone, G.; Stave, M.; Taylor, H.; Thomas, G.; Lenthe, J. v.; Wong, A.; Zhang, Z. *NWChem A Computational Chemistry Package for Parallel Computers*; Version 4.5 ed.; Pacific Northwest National Laboratory: Richland, WA, 2003.

(54) Frisch, M. J.; Trucks, G. W.; Schlegel, H. B.; Scuseria, G. E.; Robb, M. A.; Cheeseman, J. R. ; Montgomery, J. A., Jr.; Vreven, T.; Kudin, K. N.; Burant, J. C.; Millam, J. M.; Iyengar, S. S.; Tomasi, J.; Barone, V.; Mennucci, B.; Cossi, M.; Scalmani, G.; Rega, N.; Petersson, G. A.; Nakatsuji, H.; Hada, M.; Ehara, M.; Toyota, K.; Fukuda, R.; Hasegawa, J.; Ishida, M.; Nakajima, T.; Honda, Y. ; Kitao, O.; Nakai, H.; Klene, M.; Li, X.; Knox, J. E.; Hratchian, H. P.; Cross, J. B.; Adamo, C.; Jaramillo, J.; Gomperts, R.; Stratmann, R. E.; Yazyev, O.; Austin, A. J.; Cammi, R.; Pomelli, C.; Ochterski, J. W.; Ayala, P. Y.; Morokuma, K.; Voth, G. A.; Salvador, P.; Dannenberg, J. J.; Zakrzewski, V. G.; Dapprich, S.; Daniels, A. D.; Strain, M. C.; Farkas, O.; Malick, D. K.; Rabuck, A. D.; Raghavachari, K.; Foresman, J. B.; Ortiz, J. V.; Cui, Q.; Baboul, A. G.; Clifford, S.; Cioslowski, J.; Stefanov, B. B.; Liu, G.; Liashenko, A.; Piskorz, P.; Komaromi, I.; Martin, R. L.; Fox, D. J.; Keith, T.; Al-Laham, M. A.; Peng, C. Y.; Nanayakkara, A.; Challacombe, M.; Gill, P. M. W.; Johnson, B.; Chen, W.; Wong, M. W.; Gonzalez, C.; Pople, J. A. *Gaussian 03, revision B.02; Gaussian, Inc.*: Pittsburgh, PA, 2003.

(55) Montgomery, J. A., Jr.; Frisch, M. J.; Ochterski, J. W.; Petersson, G. A. *J. Chem. Phys.* **1999**, *110*, 2822.

(56) Boys, S. F.; Bernardi, R. *Mol. Phys.* **1970**, *19*, 553.

(57) van Duijneveldt, F. B.; van Duijneveldt de Rijdt, J. G. C. M.; van Lenthe, J. H. *Chem. Rev.* **1994**, *94*, 1873.

(58) Wong, C. H. S.; Siu, F. M.; Ma, N. L.; Tsang, C. W. *THEOCHEM* **2002**, *588*, 9.

(59) Feller, D.; Glendening, E. D.; Woon, M. W.; Feyereisen, J. *J. Chem. Phys.* **1995**, *103*, 3526.

(60) Feller, D. *Chem. Phys. Lett.* **2000**, *322*, 543.

(61) Lifshitz, C. *Adv. Mass Spectrom.* **1989**, *11A*, 713–729.

(62) Finch, P. *Carbohydrates: Structures, Syntheses and Dynamics*; Kluwer Academic Publishers: Netherlands, 1999.

(63) Angyal, S. J. *Adv. Carbohydr. Chem. Biochem.* **1984**, *42*, 15.

(64) Franks, F. *Pure Appl. Chem.* **1987**, *59*, 1189.

(65) El-KhademH. S. *Carbohydrate Chemistry: Monosaccharides and Their Oligomers*; Academic: San Diego, 1988.

(66) Heaton, A. L.; Moision, R. M.; Armentrout, P. B. *J. Phys Chem. A* **2008**, *112*, 3319.

JP804113Q